Theoret. Comput. Fluid Dynamics (1998) 11: 237–250

Theoretical and Computational Fluid Dynamics

Perturbation Structure and Spectra in Turbulent Channel Flow*

Brian F. Farrell

Department of Earth and Planetary Sciences,
Harvard University, Cambridge, MA 02138, U.S.A.

Petros J. Ioannou

Department of Physics,
National and Capodistrian University of Athens, Athens, Greece

Communicated by J.R. Herring

Received 30 January 1997 and accepted 27 March 1998

Abstract. The strong mean shear in the vicinity of the boundaries in turbulent boundary layer flows preferentially amplifies a particular class of perturbations resulting in the appearance of coherent structures and in characteristic associated spatial and temporal velocity spectra. This enhanced response to certain perturbations can be traced to the nonnormality of the linearized dynamical operator through which transient growth arising in dynamical systems with asymptotically stable operators is expressed. This dynamical amplification process can be comprehensively probed by forcing the linearized operator associated with the boundary layer flow stochastically to obtain the statistically stationary response.

In this work the spatial wave-number/temporal frequency spectra obtained by stochastically forcing the linearized model boundary layer operator associated with wall-bounded shear flow at large Reynolds number are compared with observations of boundary layer turbulence. The verisimilitude of the stochastically excited synthetic turbulence supports the identification of the underlying dynamics maintaining the turbulence with nonnormal perturbation growth.

1. Introduction

At high Reynolds number turbulent pipe and channel flows develop a region of strong shear adjacent to no-slip surfaces. This boundary layer supports characteristic coherent structures which are commonly described as streamwise streaks or streamwise vortices. The existence of boundary layer streaks has been recognized for some time (Kline and Runstadler, 1959; Kline *et al.*, 1967; Bakewell and Lumley, 1967) and the central role of these structures in the energetics maintaining the turbulent state has also been recognized (Kim *et al.*, 1971). Nevertheless, while morphological aspects of these coherent structures are known with some certainty, including the streak spacing of approximately $z^+ \approx 100$ (where cross-stream distance is expressed in viscous wall units) and the streamwise extent of $x^+ \approx 600$ (Smith and Metzler, 1983) and there even exist frequency/wave-number spectra of the streamwise velocity perturbations at various distances from the

* Petros J. Ioannou was supported by NSF ATM-96-25453. Brian Farrell was partially supported by NSF ATM-96-25453. This work was done at the National Center for Atmospheric Research, Mesoscale and Microscale Meteorology Division. Hospitality extended by Richard Rotunno is gratefully acknowledged. The National Center for Atmospheric Research is supported by the National Science Foundation.

wall (Morrison and Kronauer, 1969; Morrison *et al.*, 1971), there has been little success until recently in reconciling these observations with theory.

Benney and Lin (1960) suggested that Tollmien–Schlichting (T-S) waves interact nonlinearly with superimposed three-dimensional waves to produce longitudinal eddies but their mechanism failed to produce the observed spanwise wavelength and required existence of well-developed T-S waves which are not seen in fully developed boundary layer turbulence. Moreover, the mechanism of streak formation is generally accepted to be the linear process of advection of mean streamwise momentum by streamwise roll perturbations. This view is supported by comparison of structures arising in fully nonlinear direct numerical simulations with those arising from random initial conditions using the linearized equations (Lee *et al.*, 1990).

Görtler (1940) instability has been cited as a possible explanation for streamwise vortices from time to time but that instability requires a concave boundary that does not occur except perhaps transiently or as a local approximation to the background flow. More promising is the theory of Ellingsen and Palm (1975) and Landahl (1980) which describes a kinematic mechanism for producing streaks in shear flows from streamwise vortices that is not associated with an exponential instability. Benney and Gustavsson (1981) later showed that large transient growth of streaks could occur in a manner similar to that described by Landahl near a point of resonance between a Squire mode and an Orr–Sommerfeld (O-S) mode of the O–S equations. Butler and Farrell (1992) (hereafter B&F) showed that streaks are the disturbances resulting from the initial perturbation producing largest growth in shear flow and that this growth occurs even far from Squire/O–S resonance. This result implies that streaks arise naturally from small random disturbances and explains the ubiquity of streaks in shear flow. The mechanism responsible for selecting the $z^+ \approx 100$ spanwise spacing of the sublayer streaks was subsequently clarified by Butler and Farrell (1993). Their results were obtained making use of optimal perturbation theory which provides a constructive method for finding the perturbation with the greatest increase in energy over a specified interval of time (B&F). The essential additional physically based parameter used by Butler and Farrell (1993) is this interval of time which is chosen to be the decorrelation time in the flow as estimated from the observed eddy turnover time. Using this parametrization the observed streak structure is found to correspond closely with the most amplified perturbation when the appropriate Reynolds–Tiederman boundary layer profile is taken.

Optimal perturbation theory provides a method for identifying a complete orthogonal set of perturbations ordered in potential for growth as measured in a chosen norm. This theory is appropriate for identifying initial conditions conducive to growth and for placing bounds on the potential for growth as well as for predicting the structures that arise transiently in the flow (see Farrell, 1988; B&F; Reddy and Henningson, 1993; Trefethen *et al.*, 1993; Farrell and Ioannou, 1993a,b). Moreover, recognition of the potential for growth of a subset of favorably configured perturbations in strongly sheared flows leads naturally to the idea that maintenance of perturbation variance can be traced to amplification of a subset of transiently growing perturbations which are continually replenished by nonlinear wave/wave interactions (Farrell and Ioannou, 1993,d, hereafter F&I).

While optimal perturbation theory has led to insights into mechanisms of perturbation growth, it is not ideally suited for studying the statistical properties of the ensemble of all perturbations making up the turbulent flow. For this purpose the stationary statistics of the associated nonnormal dynamical system needs to be obtained and the appropriate method for accomplishing this is the theory of stochastic differential equations (F&I; Farrell and Ioannou, 1994a). Previously, stochastic analysis was applied to the study of bypass transition by demonstrating very rapid increase in variance ($O(R^3)$) with shear based Reynolds number in stochastically excited shear flows which led to a successful prediction of observed transition Reynolds numbers (Farrell and Ioannou, 1994a). A theory based on the dynamics of nonnormal operators has also successfully accounted for maintenance of the large-scale variance in the atmosphere and reproduced the observed synoptic and planetary scale wave spectra and eddy transports (Farrell and Ioannou, 1993c; 1994b; 1995).

While the methods familiar in the study of coupled stochastic differential equations associated with normal operators (see Wang and Uhlenbeck, 1945) are easily extended to the nonnormal system arising from the highly sheared flow of the turbulent boundary layer, the implications of these results are often novel (F&I). Application of methods of stochastic analysis to the mean velocity profile associated with turbulent shear flow, identifies the statistical properties of the turbulence including the Karhunen–Loeve functions that most efficiently characterize the structures accounting for the disturbance variance as well as the forcing perturbations most effective in producing the variance (F&I). Perhaps the results of most interest

for the present purposes are the spectra relating frequency and wave number in boundary layer turbulence. Such spectra have been obtained for the quasi-geostrophic turbulence of the midlatitude atmospheric jet and found to compare well with observations (Farrell and Ioannou, 1994b, 1995). Analogous to the observed atmospheric spectra are the observed spectra of streamwise velocity perturbations in the sublayer of channel flows which have been studied using hot wire anemometry (Morrison and Kronauer, 1969; Morrison *et al.*, 1971). These observations provide a more complete description of the coherent boundary layer motions than that provided by streak spacing alone.

In this work the parameterization of finite time disruption exploited in Butler and Farrell, (1993) and Farrell and Ioannou (1993a) to obtain the coherent structures in the boundary layer is extended to obtain the boundary-layer-frequency/wave-number spectra of Morrison and Kronauer (1969). To this purpose a method of accounting for the finite time correlation of disturbances in stochastically forced boundary layer flow is developed and the success of the resulting simulation of boundary layer turbulence provides support for a mechanistic theory of turbulence based on the properties of the highly nonnormal dynamical operator arising in strong shear.

2. Stochastic Dynamics of the Linearised Navier–Stokes Equations

2.a. Formulation

Consider a turbulent channel flow driven by a constant pressure gradient with streamwise (x) mean velocity $U(y)$ varying only in the cross-stream direction (y). The evolution of harmonic perturbations with streamwise wave number k_x and spanwise (z) wave number k_z are modeled by the stochastically forced linearized three-dimensional Navier–Stokes equation with a random forcing ε assumed for simplicity to be a spatially and temporally δ-correlated Gaussian white-noise process with zero mean and unit variance. The forced equation takes the form (see F&I):

$$\frac{\mathrm{d}\varphi}{\mathrm{d}t} = \mathcal{A}\varphi + \varepsilon(t), \tag{1}$$

where $\varphi = [\hat{v}\ , \hat{\eta}]^T$, with the cross-stream (y) perturbation velocity given by

$$v = \hat{v}(y,t)\ \mathrm{e}^{i(k_x x + k_z z)}, \tag{2a}$$

and the cross-stream perturbation vorticity by

$$\eta = \hat{\eta}(y,t)\ \mathrm{e}^{i(k_x x + k_z z)}, \tag{2b}$$

and in which the real parts are accorded physical interpretation.

The evolution operator can be expressed in the form

$$\mathcal{A} = \begin{bmatrix} \mathcal{L} & 0 \\ \mathcal{C} & \mathcal{S} \end{bmatrix}, \tag{3}$$

in which $\mathcal{L}$ is the O–S operator, $\mathcal{S}$ is the Squire operator, and $\mathcal{C}$ is the coupling between cross-stream vorticity and velocity resulting from the tilting of mean spanwise vorticity by the perturbation cross-stream velocity. In detail:

$$\mathcal{L} = \Delta^{-1}(-ik_x U\Delta + ik_x \mathrm{d}^2U/\mathrm{d}y^2 + \Delta\Delta/R), \tag{4a}$$

$$\mathcal{S} = -ik_x U + \Delta/R, \tag{4b}$$

$$\mathcal{C} = -ik_z \mathrm{d}U/\mathrm{d}y. \tag{4c}$$

The Laplacian operator is given by $\Delta \equiv \mathrm{d}^2/\mathrm{d}y^2 - K^2$, where K is the total horizontal wave number: $K^2 \equiv k_x^2 + k_z^2$. The operator Δ^{-1} in (4.a) is rendered unique by incorporation of the no-slip boundary conditions at the channel walls $y = \pm 1$ which require:

$$\begin{aligned} \hat{v}(\pm 1) &= 0, \\ \left.\frac{\mathrm{d}\hat{v}}{\mathrm{d}y}\right|_{y=\pm 1} &= 0, \\ \hat{\eta}(\pm 1) &= 0. \end{aligned} \tag{5}$$

We consider a spatially discrete approximation to (2) so that the spatially continuous operators reduce to finite-dimensional matrices.

In the equations above we have nondimensionalized lengths with the channel half-width, L, velocities with the friction velocity, U_τ, and time by L/U_τ.

The Reynolds number based on the friction velocity is $R \equiv U_\tau L/\nu$. Consequently, for such a turbulent channel flow we can immediately relate the Reynolds number, R, based on the friction velocity, to the Reynolds number, R_{lam}, based on the maximum velocity attained if the flow were laminar under the same pressure gradient ($R_{\mathrm{lam}} = R^2/2$). The relationship between R and the Reynolds number, $R_{\mathrm{m}} = RU_{\mathrm{m}}/U_\tau$, based on the actual maximum velocity, U_{m}, which is often quoted in experimental work, can only be obtained, at present, from experiment (see Houssain and Reynolds, 1975).

We assume as the background flow the symmetric mean velocity profile proposed by Reynolds and Tiederman (1967):

$$U(y) = \int_{-1}^{y} \mathrm{d}y \frac{Ry}{1 + \nu_E(y)}, \qquad \text{for} \quad y \in [-1, 1], \tag{6}$$

in which the variable eddy viscosity is given by

$$\nu_{\mathrm{E}}(y) = \frac{(1 + (\frac{1}{3}\kappa R(1 - y^2)(1 + 2y^2)(1 - \mathrm{e}^{-(1-|y|)R/A}))^2)^{1/2} - 1}{2}. \tag{7}$$

The profile for $\kappa = 0.4$, $A = 30$, and $R = 180$ and 2000 is shown in Figure 1. In addition, appropriate length and time scales are introduced to resolve the region adjacent to the boundaries. Specifically, length

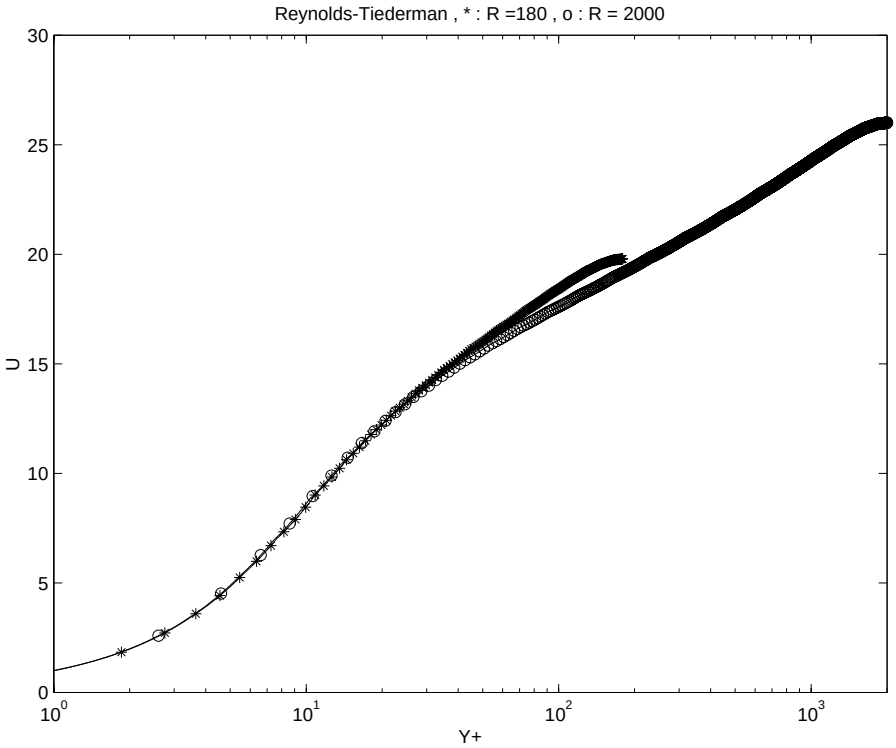

Figure 1. Mean velocity profile of the turbulent channel flow as given by the Reynolds–Tiederman equation (8) for $\kappa = 0.4$ and $A = 30$ as a function of y^+, the distance from the lower boundary. The velocity, U, is nondimensionalized by the friction velocity, U_τ. The upper curve correspond to Reynolds number $R = 180$ and the lower curve to $R = 2000$.

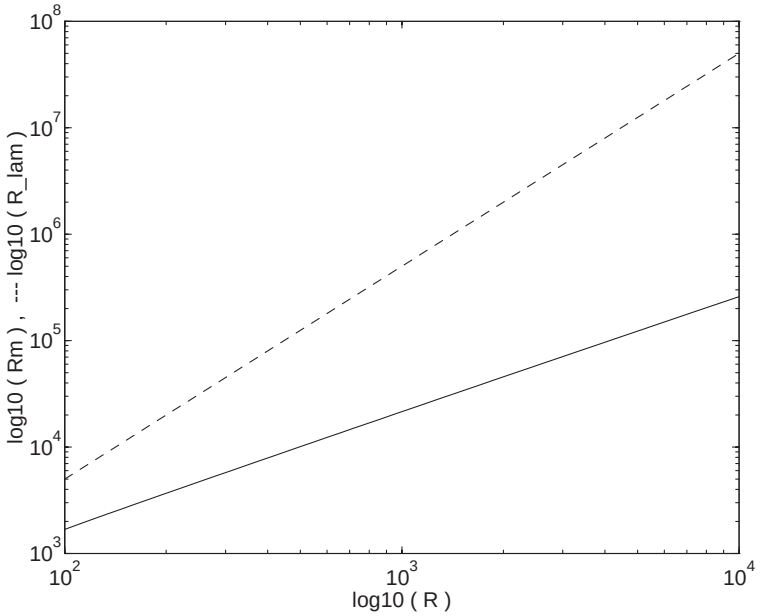

Figure 2. The Reynolds number based on the maximum velocity attained in the turbulent flow, R_{m}, as a function of the Reynolds number based on the friction velocity, R, for the Reynolds-Tiederman profile. Also (dashed line) the Reynolds number, R_{lam}, based on the maximal velocity that would be attained if the flow were maintained laminar.

is expressed in wall units ν/U_τ, and time in units of the viscous time scale ν/U_τ^2. In what follows lengths expressed in wall units and times expressed in viscous time units will be denoted with superscript +.

The Reynolds–Tiederman velocity profile gives the maximum mean velocity, U_{m}, which is attained at the center of the channel. The relationship for this Reynolds–Tiederman profile among the Reynolds number based on the friction velocity, R, the Reynolds number based on the maximum mean velocity attained in the turbulent flow, R_{m}, and the Reynolds number based on the maximal velocity that would be attained if the flow were maintained laminar, R_{lam}, are shown in Figure 2.

2.b. Determining the Temporal Evolution of Second Order Moments Under Stochastic Excitation

The forced solution of (1) is given by

$$\varphi^t = \int_0^\infty \mathrm{e}^{\mathcal{A}(t-s)}\, H(t-s)\varepsilon(s)\,\mathrm{d}s\,, \tag{8}$$

where $H(t)$ denotes the Heaviside function and the forcing is considered to be switched on at $t = 0$.

All the second-order moments of perturbation variables at time t can be found from the correlation matrix of the state vector:

$$C_{ij}^t = \langle \varphi(t)_i \varphi(t)_j^* \rangle. \tag{9}$$

In which $\langle\ \rangle$ denotes an ensemble average, a star denotes complex conjugation and indices denote a variable at the discretized level. For example φ_i for a discretization of N points corresponds to the cross-stream velocity $\hat{v}(y_i)$ for $1 \le i \le N$, and the cross-stream vorticity $\hat{\eta}(y_{i-N})$ for $N + 1 \le i \le 2N$.

Consider the ensemble average total kinetic energy. We can write the perturbation kinetic energy as

$$E^t = \varphi^\dagger \mathcal{M} \varphi = u^\dagger u, \tag{10}$$

where $\varphi^\dagger$ is the hermitian transpose of φ, $u = \mathcal{M}^{1/2}\varphi$ is a generalized velocity, and the energy metric is defined, for a cross-stream grid interval δy, by

$$\mathcal{M} = \frac{\delta y}{8K^2} \begin{bmatrix} -\Delta & 0 \\ 0 & \mathcal{I} \end{bmatrix}, \tag{11}$$

where $\mathcal{I}$ is the identity, and Δ is the discretized Laplacian operator (in what follows all operators are to be interpreted with their finite difference approximation). The ensemble average total energy is then given in terms of the correlation matrix $\mathcal{C}^t$ by

$$\langle E^t \rangle = \text{trace}(\mathcal{M}^{1/2}\mathcal{C}^t\mathcal{M}^{1/2}). \tag{12}$$

The correlation matrix is obtained from (8) by using the statistical properties of the noise. We have (F&I):

$$\mathcal{C}^t = \int_0^t \mathrm{e}^{\mathcal{A}(t-s)}\mathrm{e}^{\mathcal{A}^\dagger(t-s)}\,\mathrm{d}s. \tag{13}$$

To obtain the evolution equation for $\mathcal{C}^t$, note that $\mathcal{C}^0 = 0$ and that the statistically steady state is convergent to the time-independent correlation matrix, $\mathcal{C}^\infty$, if the dynamics are asymptotically stable. Time differentiation of (13) immediately gives an equation for the temporal evolution of $\mathcal{C}^t$:

$$\frac{d\mathcal{C}^t}{dt} = \mathcal{I} + \mathcal{A}\mathcal{C}^t + \mathcal{C}^t\mathcal{A}^\dagger, \tag{14}$$

which can be solved for the time dependence of the correlation matrix:

$$\mathcal{C}^t = \mathcal{C}^\infty - \mathrm{e}^{\mathcal{A}t}\mathcal{C}^\infty\,\mathrm{e}^{\mathcal{A}^\dagger t}, \tag{15}$$

in which the asymptotic correlation matrix $\mathcal{C}^\infty$ which characterizes the statistically steady state is determined from solution of the Liapunov equation:

$$\mathcal{A}\mathcal{C}^\infty + \mathcal{C}^\infty\mathcal{A}^\dagger = -\mathcal{I}, \tag{16}$$

which can in turn be solved with standard methods.

2.c. Determining the Frequency Spectrum of the Maintained Variance

Consider the Fourier transform pair:

$$\varphi(t) = \int_{-\infty}^{\infty} \hat{\varphi}(\omega)\,\mathrm{e}^{i\omega t}\,\mathrm{d}\omega. \tag{17a}$$

$$\hat{\varphi}(\omega) = \frac{1}{2\pi}\int_{-\infty}^{\infty} \varphi(t)\,\mathrm{e}^{-i\omega t}\,\mathrm{d}t. \tag{17b}$$

Applying the convolution theorem to (8) we obtain

$$\hat{\varphi}(\omega) = \mathcal{R}(\omega)\hat{\varepsilon}(\omega) \tag{18}$$

with resolvent

$$\mathcal{R}(\omega) = (i\omega\mathcal{I} - \mathcal{A})^{-1}. \tag{19}$$

The steady state streamwise velocity variance at y_i is

$$\langle u_i u_i^* \rangle = \int_{-\infty}^{\infty}\int_{-\infty}^{\infty} \mathcal{U}_{ia}\mathcal{R}_{ab}(\omega)\langle\hat{\varepsilon}_b(\omega)\hat{\varepsilon}_{\mathrm{m}}^*(\omega')\rangle\mathcal{U}_{il}^*\mathcal{R}_{lm}^*(\omega')\,\mathrm{e}^{i(\omega-\omega')t}\,\mathrm{d}\omega\,\mathrm{d}\omega', \tag{20}$$

in which there is no summation over i implied and in which the operator $\mathcal{U}$ is defined as

$$\mathcal{U} = \frac{i}{K^2}\begin{bmatrix} k_x(\mathrm{d}/\mathrm{d}y) & 0 \\ 0 & -k_z \end{bmatrix}. \tag{21}$$

Assuming unit white noise forcing characterized by

$$\langle\hat{\varepsilon}_k(\omega)\hat{\varepsilon}_{\mathrm{m}}^*(\omega')\rangle = \frac{1}{2\pi}\delta_{km}\delta(\omega-\omega'), \tag{22}$$

we have from (20)

$$\langle |u_i|^2 \rangle = \frac{1}{2\pi} \int_{-\infty}^{\infty} \Phi_{ii}(\omega)\, \mathrm{d}\omega, \tag{23}$$

in which the energy spectrum associated with a particular level in the cross-stream direction is given by the diagonal element of

$$\Phi(\omega) = \mathcal{U}\mathcal{R}(\omega)\mathcal{R}^{\dagger}(\omega)\mathcal{U}^{\dagger}. \tag{24}$$

2.d. The Role of Finite Coherence Time in Shear Turbulence

Transient growth in shear flow is most effectively produced when two generic mechanisms occur in combination: an initial upstream shearing in the streamwise–cross-stream plane that rapidly amplifies the cross-stream velocity (essentially the two-dimensional mechanism identified by Orr (1907)), followed by sustained growth of the streamwise velocity by cross-stream advection of the background streamwise velocity which results in the production of streaks (the mechanism identified by Moffat (1967), Ellingsen and Palm (1975) and Landahl (1980)). These two mechanisms operate symbiotically in shear flows producing perturbations of universal form that to good approximation depend on the flow only through the time interval over which this growth process proceeds. This time interval is conveniently scaled by a representative shear, i.e., on $S^* = T_{\mathrm{opt}}(\mathrm{d}U/\mathrm{d}y)$ (Farrell and Ioannou, 1993a). For large S^*, i.e., $S^* > 20$, the optimal perturbations are streamwise rolls. With decreasing S^* the optimal perturbations become increasingly oblique, thereby taking advantage of the rapid but short-lived Orr mechanism, and as a result assume the form of double roller eddies (Townsend, 1972).

In boundary layer flow the shear is typically highly concentrated near the boundary and the extent of the interval of growth combines with the boundary constraint to affect the optimal perturbation structure. For small optimizing times perturbations assume small scale in order to exploit the region of maximum S^* near the ground. For larger optimizing times the viscous decay which is proportional to the square of the wave number results in retreat of the optimals to larger scale. In boundary layer flow the compromise between these two influences produces optimal perturbation typically found to have $k_x \approx 0$ and $k_z \approx 0.5$–2 in conjunction with maximal energy amplification of $E^t/E^0 \approx R^2$ at time $t \approx R$ over a wide range of Reynolds numbers (B&F; Reddy and Henningson, 1993; Trefethen *et al.*, 1993; Farrell and Ioannou 1993a,b). The effect of wave number on the growth of perturbations is shown in Figure 3 for a turbulent channel flow with $R = 180$. The perturbation with spanwise wave number $k_z = 10$ (corresponding to the observed streak spacing $\lambda_z^+ = 100$) produces rapid initial growth, but because of dissipation does not exhibit growth for $T_{\mathrm{opt}} > 2$. The maximal growth for this disturbance is attained for $T_{\mathrm{opt}} \approx 0.5$ which corresponds when expressed in wall units to $T_{\mathrm{opt}}^+ \approx 90$ which as we will see is the eddy turnover time appropriate for the sublayer region.

The growth of a given perturbation in turbulent flow cannot continue to arbitrary time because of disruption by other perturbations and we assume that this time is set by the coherence time of the turbulent flow approximated by the eddy turnover time, T_{e}. The structure of the optimal perturbations depends on the eddy turnover time, T_{e}, expressed in local shear time units, *i.e.* on $S^* = dU/dyT_{\mathrm{e}}$. The importance of this nondimensional interval was recognized by Lee *et al.* (1990) who provide estimates which are shown in Figure 4. Butler and Farrell (1993) showed that the perturbations in the turbulent sublayer that optimize energy in an eddy turnover time characteristic of sublayer turbulence have the observed $z^+ = 100$ streak spacing.

In order to model the stochastic response of the turbulent flow accurately we must ensure that variance is not allowed to accumulate over times longer than typical coherence times. In Figure 5 we show the development of the ensemble perturbation energy as a function of time for the same wave numbers for which the transient growth potential was shown in Figure 3.

2.f. Incorporating Finite Coherence Time in the Stochastic Calculus

The effect of finite coherence time on the evolution of disturbances is modeled by assuming that the perturbation field is disrupted and set to zero after an interval, T_{c}, following its excitation by the forcing.*

* The observed spectra of transient disturbances in the midlatitude atmosphere can be modeled by restricting the persistence of motions solely through the choice of an effective level of dissipation. This relatively simple parametrization of eddy effects succeeds presumably because the variance is dominated by stable modes (Farrell and Ioannou, 1995). In the present case of turbulent channel flows explicit incorporation of the coherence time in the manner described proved to model the spectra more accurately.

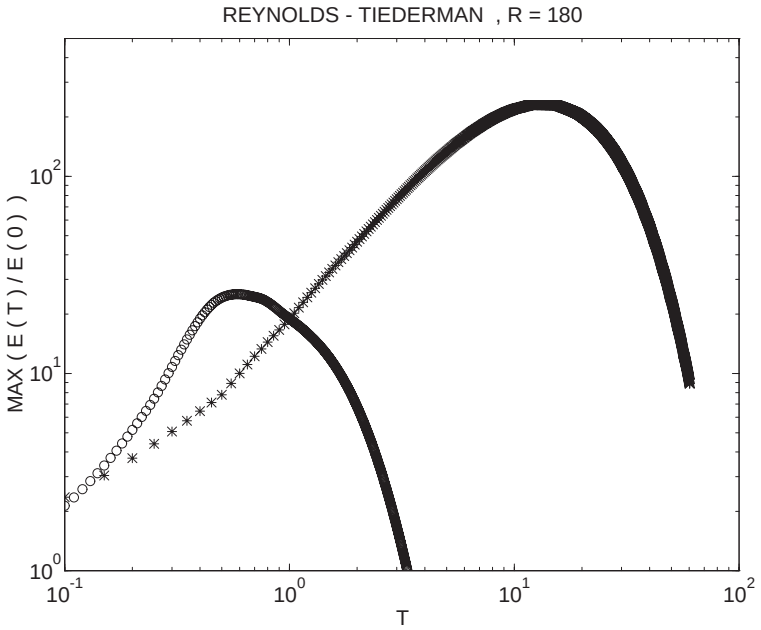

Figure 3. Energy growth of the optimal perturbation as a function of optimizing time, $T_{\rm opt}$, for $\lambda_z^+ = 100$ ($k_z = 11.3$), $\lambda_x^+ = 600$ ($k_x = 1.88$) (circles), and for the global optimal $k_x = 0$, $\lambda_z^+ = 565$ ($k_z = 2$) (stars). The background velocity is shown in Figure 1 and the Reynolds number is $R = 180$. The maximal energy growth can be found by calculating the L_2 norm of $\mathrm{e}^{\mathcal{M}^{1/2}\mathcal{A}\mathcal{M}^{-1/2}T}$, where $\mathcal{A}$ is the evolution operator and $\mathcal{M}$ is the energy metric given by (11.).

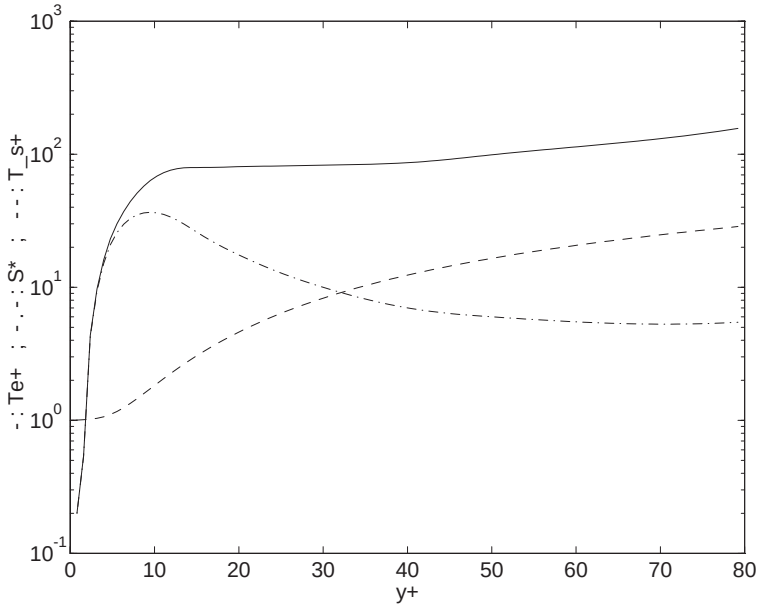

Figure 4. Eddy turnover time $T_{\rm e}^+$ (continuous line) as a function of distance from the wall (y^+) in turbulent channel flow, as estimated from the values of the shear rate parameter $S^* = T_{\rm e} dU/dy$ (dot-dash line) obtained by Lee *et al.* (1990). The dashed curve gives the shear time $T_s^+ = 1/(dU/dy^+)$ calculated from the Reynolds–Tiederman velocity profile. Note that S^* has a peak of 35 at ≈ 10 wall units which results in streamwise vortices becoming the associated optimals, and asympotes to a value of ≈ 5 in the logarithmic layer which results in double roller eddies becoming the associated optimal disturbances.

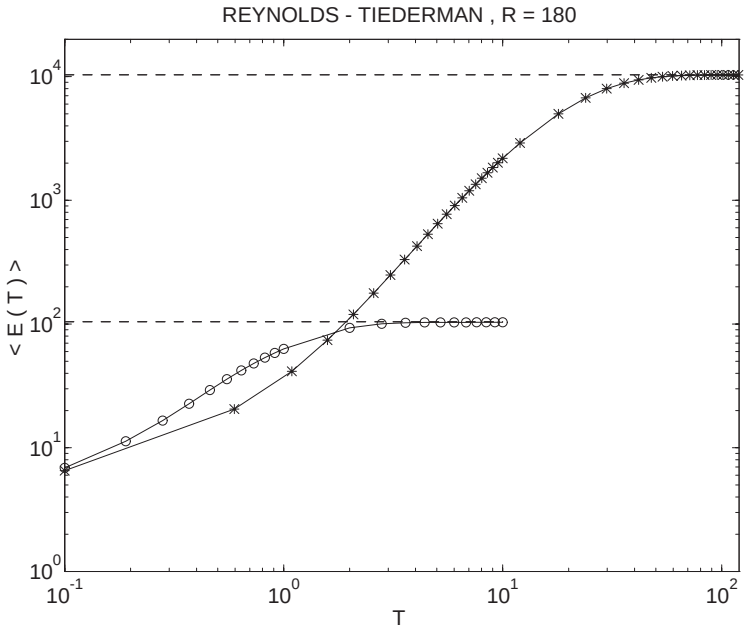

Figure 5. Time development of the ensemble average perturbation energy for $\lambda_z^+ = 100$ ($k_z = 11.3$), $\lambda_x^+ = 600$ ($k_x = 1.88$) (circles), and for the global optimal which occurs at $k_x = 0$, $\lambda_z^+ = 565$ ($k_z = 2$) (stars). The corresponding time in wall units is $T^{+} = RT$. The background velocity is shown in Figure 1.

The perturbation field takes the form:

$$\varphi^t = \int_0^\infty \mathrm{e}^{\mathcal{A}(t-s)}\, H(t-s) S^{T_\mathrm{c}}(t-s)\varepsilon(s) ds, \tag{25}$$

with

$$S^{T_\mathrm{c}}(t-s) = (1 - H(t-s-T_\mathrm{c})). \tag{26}$$

Consider the correlation matrix $\mathcal{C}_{ij}^{T_\mathrm{c}} = \langle \varphi_i^t \varphi_j^{t*} \rangle$ valid for times $t \geq T_\mathrm{c}$:

$$\mathcal{C}_{ij}^{T_\mathrm{c}} = \int_0^t \mathrm{e}_{ia}^{\mathcal{A}(t-s)}\, \mathrm{e}_{aj}^{\mathcal{A}^\dagger(t-s)} S^{T_\mathrm{c}}(t-s)\, \mathrm{d}s \tag{27a}$$

$$= \int_{T_\mathrm{c}-t}^{T_\mathrm{c}} \mathrm{e}_{ia}^{\mathcal{A}(T_\mathrm{c}-x)}\, \mathrm{e}_{aj}^{\mathcal{A}^\dagger(T_\mathrm{c}-x)} (1 - H(-x))\, \mathrm{d}x \tag{27b}$$

$$= \int_0^{T_\mathrm{c}} \mathrm{e}_{ia}^{\mathcal{A}(T_\mathrm{c}-x)}\, \mathrm{e}_{aj}^{\mathcal{A}^\dagger(T_\mathrm{c}-x)}\, \mathrm{d}x \tag{27c}$$

where $x = s - t + T_\mathrm{c}$. Comparing (27c) to (13) it can be seen that the variance of the disrupted boundary layer is obtained by accumulating the variance over the interval of time T_c. Comparing with (15) we have for the disrupted flow a correlation matrix given by

$$\mathcal{C}^{T_\mathrm{c}} = \mathcal{C}^\infty - \mathrm{e}^{\mathcal{A}T_\mathrm{c}} \mathcal{C}^\infty \mathrm{e}^{\mathcal{A}^\dagger T_\mathrm{c}}, \tag{28}$$

from which, as previously remarked, we can obtain all the statistics of the flow.

To obtain the frequency spectrum for a turbulent flow with coherence time T_c we proceed as in Section 2.c. The Fourier transform of (25) produces the finite T_c resolvent

$$\mathcal{R}^{T_\mathrm{c}}(\omega) = \mathcal{R}(\omega)\mathcal{F}, \tag{29}$$

which is the product of the resolvent for the undisrupted flow given in (19) and the filter:

$$\mathcal{F} = \mathcal{I} - \mathrm{e}^{-(i\omega\mathcal{I} - \mathcal{A})T_\mathrm{c}} \tag{30}$$

which due to the asymptotic stability of $\mathcal{A}$ reduces to the identity for large T_c and approaches the inverse of the resolvent multiplied by T_c for small T_c, so that in this limit the spectrum becomes white.

The corresponding frequency spectrum of the streamwise velocity variance is given by

$$\Phi^{T_c}(\omega) = \mathcal{U}\mathcal{R}^{T_c}(\omega)\mathcal{R}^{T_c\dagger}(\omega)\mathcal{U}^\dagger. \tag{31}$$

3. An Example of Perturbation Spectra in the Turbulent Sublayer

For a flow with $R = 250$ the maintained ensemble average energy as a function of spanwise wave number k_z^+ for streamwise rolls with coherence times $T_c^+ = 30, 60, 90, 120, 150$ is shown in Figure 6. The response for $T_c = 90$ is as in Smith and Metzler (1983) (see Kline *et al.* 1967; Johansson *et al.* 1991) with a peak at the observed spanwise spacing of $z^+ \approx 100$. Consequently we select the value of $T_c = 90$ for our simulations.

Detailed spectra of sublayer turbulence have been obtained from experiments at high Reynolds numbers (R = 500–2000) by Morrison and Kronauer (1969) and Morrison *et al.* (1971). They obtained the power spectrum of the streamwise velocity variance $\langle |u|^2 \rangle$ at various distances from the wall as a function of streamwise and spanwise wave number by Fourier transforming the observed temporal and spatial correlation functions. They then displayed the normalized spectral densities as a function of log frequency and log wave number and in order that equal spectral power be represented by equal area in the logarithmic plot they introduced the auxiliary spectral densities:

$$\begin{aligned} \mathcal{P}(\omega^+, k_z^+) &= \omega^+ k_z^+ \Phi^{T_c}(\omega^+, k_z^+), \\ \mathcal{P}(\omega^+, k_x^+) &= \omega^+ k_x^+ \Phi^{T_c}(\omega^+, k_x^+), \end{aligned} \tag{32}$$

with the following property:

$$\int_0^\infty \int_0^\infty \Phi^{T_c}(\omega^+, k_z^+)\, \mathrm{d}\omega^+\, \mathrm{d}k_z^+ = \int_0^\infty \int_0^\infty \mathcal{P}(\omega^+, k_z^+)\, \mathrm{d}(\log(\omega^+))\, \mathrm{d}(\log(k_z^+)), \tag{33a}$$

$$\int_0^\infty \int_0^\infty \Phi^{T_c}(\omega^+, k_x^+)\, \mathrm{d}\omega^+\, \mathrm{d}k_x^+ = \int_0^\infty \int_0^\infty \mathcal{P}(\omega^+, k_x^+)\, \mathrm{d}(\log(\omega^+))\, \mathrm{d}(\log(k_x^+)). \tag{33b}$$

We adopt this convention in order to facilitate comparison.

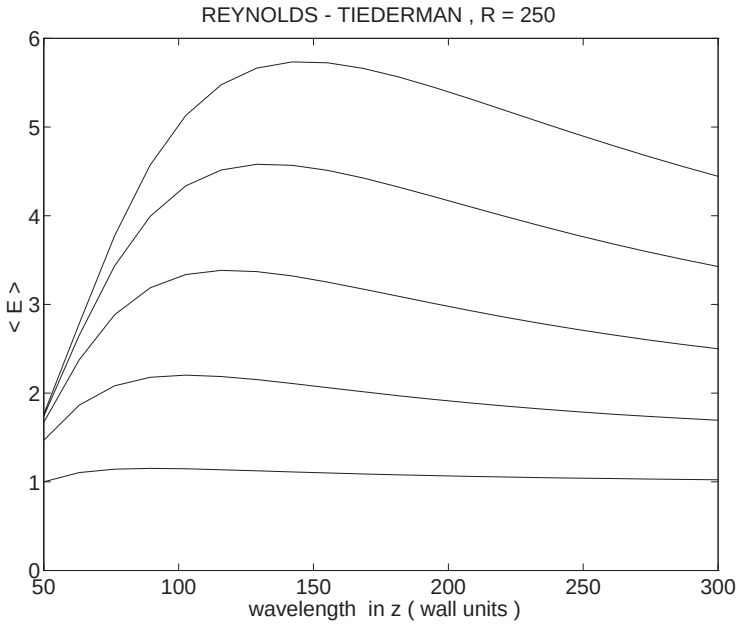

Figure 6. The statistically steady ensemble average energy for a flow with $R = 250$ as a function of spanwise wavelength λ_z^+ and for streamwise rolls with coherence times $T_c^+ = 30, 60, 90, 120, 150$ (the curves correspond to the coherence times in ascending order from bottom to top).

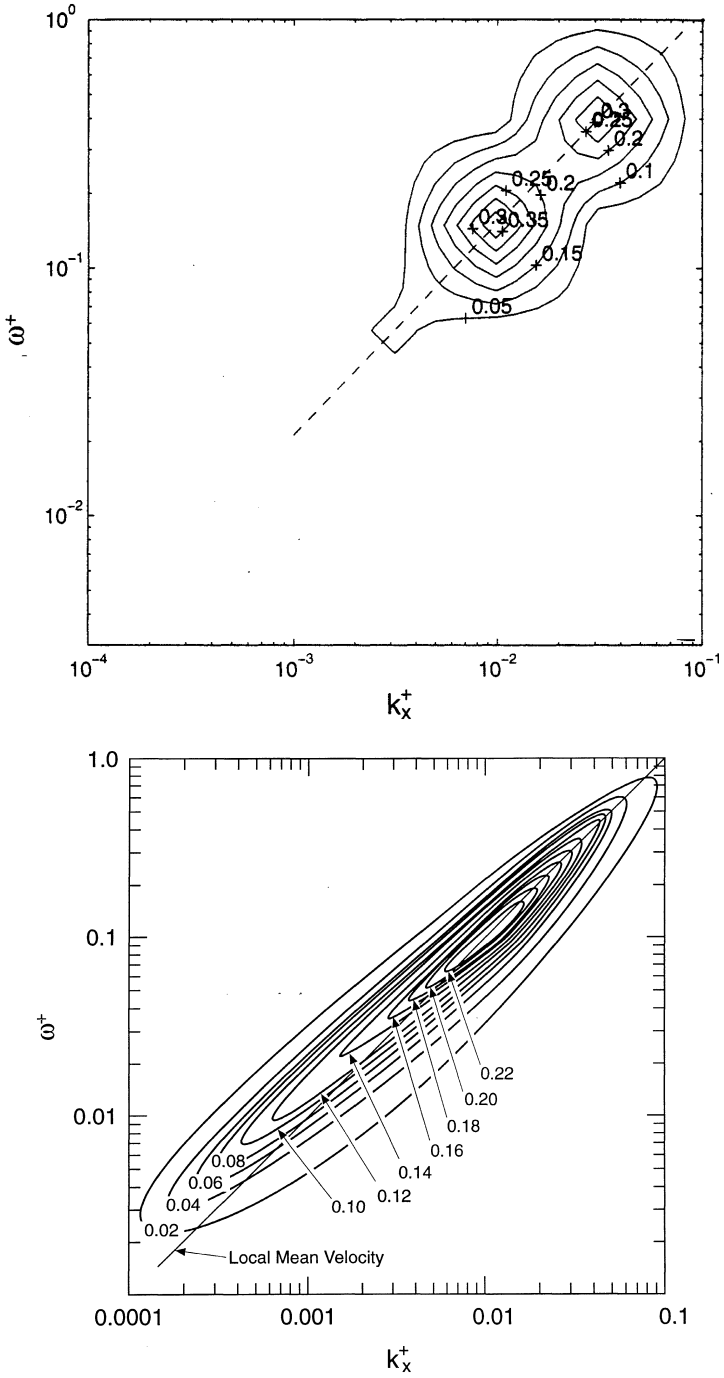

Figure 7. (a) Contours of $\log_{10} \mathcal{P}(\omega^+, k_x^+)$ at $y^+ = 13.8$ as a function of $\log_{10} k_x^+$ and $\log_{10} \omega^+$ for $\lambda_z = 130$. The coherence time is $T_c^+ = 90$ and the friction velocity based Reynolds number is $R = 2000$ which corresponds to a Reynolds number based on the actual maximum velocity of $R_m \approx 41\,000$. The straight line corresponds to a mean velocity $U^+ = 10$. (b) Contours of normalized $\mathcal{P}(\omega^+, k_x^+)$ at $y^+ = 14.6$ as a function of k_x^+ and ω^+ for a flow with $R_m = 45\,600$ as obtained experimentally by Morrison and Kronauer (1969) (their Figure 7(b)). The straight line corresponds to the mean velocity at $y^+ = 14.6$.

For comparison we have obtained spectral densities for a variety of Reynolds numbers by stochastic analysis, and typical results for $R = 2000$ and a representative coherence time of $T_c^+ = 90$ are shown in Figures 7(a) and 8(a) Because the variance is concentrated in the near-wall region we were able to integrate the equations at high Reynolds number by limiting the domain to the first 100 wall units and imposing a

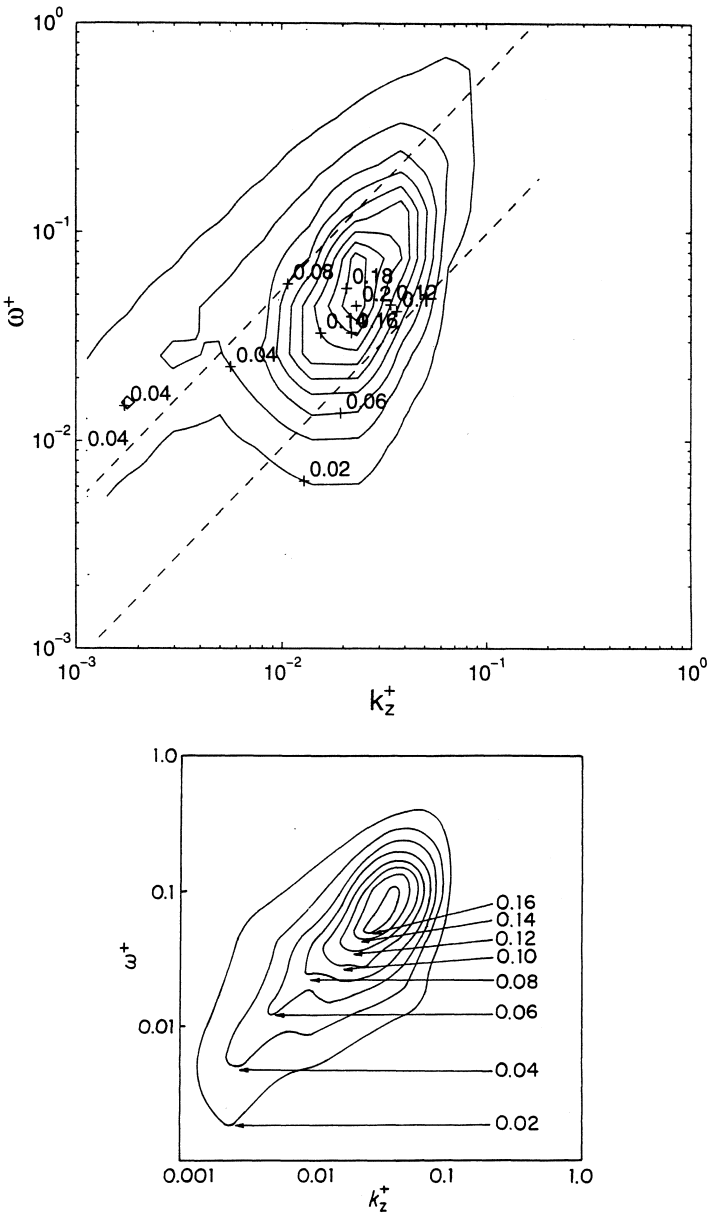

Figure 8. (a) Contours of $\log_{10} \mathcal{P}(\omega^+, k_z^+)$ at $y^+ = 7.5$ as a function of $\log_{10} k_z^+$ and $\log_{10} \omega^+$ for $\lambda_x = 600$. The coherence time is $T_c^+ = 90$ and the friction velocity based Reynolds number is $R = 2000$ which corresponds to a Reynolds number based on the actual maximum velocity of $R_m \approx 41\,000$. (b) Contours of normalized $\mathcal{P}(\omega^+, k_z^+)$ at $y^+ = 7.5$ as a function of k_z^+ and ω^+ for a flow with $R_m = 46\,400$ as obtained experimentally by Morrison, Bullock, and Kronauer (1971) (their Figure 4).

symmetry condition in the interior. We have checked the convergence of our results by doubling the size of the domain and in the case of the lower Reynolds numbers of $R = 180$ and $R = 250$ by comparison with integrations of the whole domain.

Contours of spectral density $\mathcal{P}(\omega^+, k_x^+)$ for $\lambda_z^+ = 130$ at $y^+ = 13.8$ are shown in Figure 7(a). The corresponding plot from Morrison and Kronauer (1969) is shown in Figure 7(b). The spectral density peaks for $0.05 \leq \omega^+ \leq 0.3$ and $0.01 \leq k_x^+ \leq 0.03$ and although we have limited our study to the dominant spanwise wave number the agreement is encouraging. The straight lines at 45° in Figure 7 are lines of constant phase velocity and their intersection with the ordinate $\log_{10} k_x = 1$ indicates the phase velocity which coincides with the mean velocity of the flow at the height shown *i.e.* $U = 10$. The spectral density peak gives for this location the dispersion relation $\omega^+ = 10 k_x$. This relation can be used, in the manner of Morrison *et al.* (1971),

to obtain the power density $\mathcal{P}(\omega^+, k_z^+)$ due to all wave numbers k_x. Otherwise, consideration of multiple streamwise wave numbers is necessary in the calculation of this spectrum because, as can be seen from Figure 7(a), the spectral density is not localized. We obtain the streamwise velocity variance as a function of k_x^+ and k_z^+ and then use the dispersion relation to obtain $\mathcal{P}(\omega^+, k_z^+)$. The result is shown in Figure 8(a) and for comparison the results of Morrison *et al.* (1971) are shown in Figure 8(b). Concentration of the power density at the observed 130 wall unit spanwise spacing and at the observed frequencies is verified by comparison of Figure 8(a) and 8(b).

6. Conclusions

The turbulent state of wall-bounded flows is characterized by energetic interactions between the highly sheared mean flow of the boundary layer and coherent disturbances having the form of streamwise streaks and associated streamwise vortices. Because of the very high shears found in the boundary layer, perturbation dynamics may plausibly be anticipated to be dominated by interaction between the mean shear and the perturbations which is fully incorporated in the linear dynamical operator. This fundamental linearity of boundary layer turbulence dynamics is demonstrated by comparisons performed between simulations with and without inclusion of nonlinear wave interactions (Lee *et al.*, 1990). Despite this evident simplicity of the dynamics, straightforward calculation of the eigenspectrum of the linearized dynamical operator fails to produce structures with the observed form of streamwise vortices. This failure of correspondence can be understood from the perspective of analysis of the nonnormal operator associated with the linear dynamics as due to the fact that while the perturbations of maximal growth in the linear problem take the form of streamwise rolls, these are not the eigenfunctions of the linearized operator, rather they are the optimal structures identified with the first singular vectors of the propagator arising from the dynamical operator in an appropriate norm and with an appropriate time interval for development.

A first approximation to the dominant structure in the boundary layer is suggested by the above considerations to be that structure produced by the optimal perturbation over a coherence time interval estimated to be the eddy turnover time (Butler and Farrell, 1993; Farrell and Ioannou 1993a). In this work a more comprehensive theory of the turbulent state has been developed by obtaining the spectrum of response of the dynamical operator associated with the turbulent flow through analysis of the response of the operator to stochastic excitation. Agreement with the observed boundary layer spectrum in turbulent channel flow is obtained if the accumulation of variance is restricted to an interval of time corresponding to a representative coherence time in the flow.

References

Bakewell, H.P., and Lumley, J.L. (1967) Viscous sublayer and adjacent wall region in turbulent pipe flow. *Phys. Fluids* **10**, 1880.

Benney, D.J., and Gustavsson, L.H. (1981) A new mechanism for linear and nonlinear hydrodynamic instability. *Stud. Appl. Math.* **64**, 185–209.

Benney, D.J., and Lin, C.C. (1960) On the secondary motion induced by oscillations in a shear flow. *Phys. of Fluids* **3**, 656–657.

Butler, K.M., and Farrell, B.F. (1992) Three-dimensional optimal perturbations in viscous shear flow. *Phys. Fluids A***4**, 1637–1650.

Butler, K.M., and Farrell, B.F. (1993) Optimal perturbations and streak spacing in wall-bounded turbulent shear flow. *Phys. Fluids A* **5**, 774–777.

Ellingsen, T., and Palm, E. (1975) Stability of linear flow. *Phys. Fluids* **18**, 487–488.

Farrell, B.F. (1987) Developing disturbances in shear. *J. Atmos. Sci.* **44**, 2191–2199.

Farrell, B. F. 1988: Optimal excitation of perturbations in viscous shear flow. *Phys. Fluids* **31**, 2093-2102.

Farrell, B.F., and Ioannou, P.J. (1993a) Optimal excitation of three-dimensional perturbations in viscous constant shear flow. *Phys. Fluids A***5**, 1390-1400.

Farrell, B.F., and Ioannou, P.J. (1993b) Perturbation growth in shear flow exhibits universality. *Phys. Fluids A* **5**, 2298–2300.

Farrell, B.F., and Ioannou, P.J. (1993c) Stochastic Forcing of the Navier–Stokes equations. *Phys. Fluids A* **5**, 2600–2700.

Farrell, B.F., and Ioannou, P.J. (1993d) Stochastic dynamics of baroclinic waves. *J. Atmos. Sci.* **50**, 4044–4057.

Farrell, B.F., and Ioannou, P.J. (1994a) Variance maintained by stochastic forcing of non-normal dynamical systems associated with linearly stable shear flows. *Phys. Rev. Lett.* **72**, 1188–1191.

Farrell, B.F., and Ioannou, P.J. (1994b) A theory for the statistical equilibrium energy spectrum and heat flux produced by transient baroclinic waves. *J. Atmos. Sci.* **51**, 2685–2698.

Farrell, B.F., and Ioannou, P.J. (1995) Stochastic dynamics of the midlatitude jet. *J. Atmos. Sci.***52**, 1642–1656.
Görtler, H. (1940) Über eine dreidimensionale Instabilität laminarer Grenzschichten in konkaven Wänden. *Nachr. Ges. Wiss. Göttingen, N.F.* **2**(1), 1–26.
Houssain, A.K.M.F., and Reynolds, W.C. (1975) Measurements in fully developed turbulent channel flow. *Trans. ASME Ser. I J. Fluid Engrng.* **97**, 568–578.
Ioannou, P.J. (1994) Non-normality always increases variance. *J. Atmos. Sci.* **52**, 1155–1158.
Johansson, A.V., Alfredsson, P.H., and Kim J. (1991) Evolution and dynamics of shear layer structures in near wall turbulence. *J. Fluid Mech.* **224**, 579–599.
Kim, H.T., Kline, S.J., and Reynolds W.C. (1971) The production of turbulence near a smooth wall in a turbulent boundary layer. *J. Fluid Mech.* **50**, 133–161.
Kline, S.J., and Runstadler, P.W. (1959) Some preliminary results of visual studies of wall layers of the turbulent boundary layer. *Trans. ASME Ser. E J. Appl. Mech.* **26**, 166.
Kline, S.J., Reynolds, W.C., Schraub, F.A., and Runstadler, P.W. (1967) The structure of turbulent shear layers. *J. Fluid Mech.* **30**, 741–773.
Landahl, M.T. 1980: A note on an algebraic instability of inviscid parallel shear flows. *J. Fluid Mech.* **98**, 243–251.
Lee, M.J., Kim J., and Moin P. (1990) Structure of turbulence at high shear rate. *J. Fluid Mech.* **216**, 561–583.
Moffat, H.K. (1967) The interaction of turbulence with strong shear. In *Atmospheric Turbulence and Radio Wave Propagation* A.M. Yaglom and V.I. Tatarski, eds. Nauka, Moscow, p. 139.
Morrison, W.R.B., and Kronauer, R.E. (1969) Structural similarity for fully developed turbulence in smooth tubes. *J. Fluid Mech.* **39**, 117–141.
Morrison, W.R.B., Bullock, K.J., and Kronauer, R.E. (1971) Experimental evidence of waves in the sublayer. *J. Fluid Mech.* **47**, 639–656.
Orr, W.M'F. (1907) The stability or instability of the steady motions of a perfect liquid and of a viscous liquid. *Proc. R. Irish Acad. A* **27**, 9–138.
Reddy, S.C., and Henningson, D.S. (1993) Energy growth in viscous channel flows. *J. Fluid Mech.* **252**, 209–238.
Reynolds, W.C., and Tiederman, W.G. (1967) Stability of turbulent channel flow, with application to Malkus's theory. *J. Fluid Mech.* **27**, 253–272.
Smith, C.R., and Metzler, S.P. (1983) The characteristics of low speed streaks in the near wall region of a turbulent boundary layer. *J. Fluid Mech.* **129**, 27–54.
Townsend, A.A. (1972) Entrainment and structure of turbulent flow. *J. Fluid Mech.* **41**, 13–46.
Trefethen, L.N., Trefethen, A.E., Reddy, S.C., and Driscoll, T.A. (1993) Hydrodynamic stability without eigenvalues. *Science* **261**, 578–584.
Wang, M.C., and Uhlenbeck, G.E. (1945) On the theory of Brownian motion II. *Rev. Mod. Phys.*, **17**, 323–342.